Heliyon

Received:
27 August 2018
Revised:
2 January 2019
Accepted:
30 January 2019

Cite as: Anton Jansson, Lars Pejryd. Dual-energy computed tomography investigation of additive manufacturing aluminium–carbon-fibre composite joints. Heliyon 5 (2019) e01200. doi: 10.1016/j.heliyon.2019.e01200

Dual-energy computed tomography investigation of additive manufacturing aluminium–carbon-fibre composite joints

Anton Jansson *, **Lars Pejryd**

School of Science and Technology, Örebro University, 701 82 Örebro, Sweden

* Corresponding author.
E-mail address: anton.jansson@oru.se (A. Jansson).

Abstract

In this work, aluminium–carbon-fibre reinforced plastic joints have been studied. Three types of samples were designed as double lap joints where the aluminium inserts were fabricated using both classical methods (milling) and additive manufacturing. Two versions of the joint were fabricated using additive manufacturing, one flat, and the other with small teeth designed to hook into the carbon-fibre plies. The joints were characterised using a non-linear, dual-energy computed tomography method to evaluate the bond between the composite and the metal inserts. The mechanical strength of the bonds was evaluated, both through tensile tests and four-point bending. A simple finite element model was used to discuss the joints behaviour. It was found that the joints fabricated using additive manufactured inserts were more resistant to peel stress than the milled inserts. In four-point bending tests the moment that the joint could withstand was increased by roughly 300% with the use of additive manufacturing and 400% with the use of additive manufacturing and small teeth. However, in tensile tests it was found that the teeth design reduced the maximum load capacity of the joints by roughly 30% due to porosity. Further, it was found that the additive manufactured samples did not add to the capability of withstanding shear stress. The information gained with the

https://doi.org/10.1016/j.heliyon.2019.e01200

dual-energy computed tomography method was highly valuable as the behaviour of the joints would have been difficult to explain without the porosity information.

Keywords: Mechanical engineering, Materials science

1. Introduction

The ability to join dissimilar materials is of high interest because it enables designers to freely interchange between materials to always utilize the material with the best properties for a specific part of a component. A typical situation where it is beneficial to join dissimilar materials is the joining of metals and composites. For example, in an automotive chassis it is beneficial to use carbon-fibre reinforced plastic (CFRP) where the chassis needs to be light and stiff and aluminium where the deformation needs to be controlled. When joining such materials it is usually of interest to have a joint that can transfer load between the materials without causing stress concentrations or wear on the joint. Classically these joints are fabricated with adhesives and mechanical fasteners such as screws and rivets [1, 2]. In the case of the mechanical fasteners they usually require holes to be drilled into the composite to accommodate for the fasteners. Such holes often cause stress concentrations and damage to the composite [3, 4].

There have been studies where CFRP and metals have been joined with the help of surface treatments of the metal [5]. The surface treatments aimed to produce protrusions on the metal surface that could interlace with the CFRP and create not only an adhesive but also mechanical joint between the materials. Methods that have been investigated range from laser sculpting of the metal surface, to having features cut in metal sheets that can be bent to forms surface structures [6]. The results from these studies shows varying amounts of success but the studies often have difficulties to explain what happens in the joints during loading because of the complicated interfaces.

Metal–CFRP joints have also been fabricated using additive manufacturing (AM), this enables significantly more freedom when it comes to designing of the metal. One joint, known as COMELD™, started out with laser sculpting but have lately started to use AM to produce pins that are designed to protrude into the CFRP [7]. There has also been more elaborate designs, for example a joint named “HYPER” uses pins with an arrowhead designed to prevent pull-out of the pins from the CFRP [8]. Some of the designs displayed significant improvements of the joints mechanical performance compared to joints with only adhesives [9, 10]. A drawback in all of the aforementioned designs is that they are highly limited as to how they can be fabricated by the AM process. Many of the designs can only be fabricated in the z-direction of the powder-based AM systems.

One of the difficulties when developing these type of joints is that the complex interface between the metal and CFRP is difficult to characterise. This is commonly done by cutting samples to investigate specific cross-sections, however, this method runs the risk of missing out on important information and the samples are destroyed in the process. Non-destructively, the joints are difficult to inspect as it is difficult to use common methods such as ultrasound and eddy-current on the complicated interface regions [11, 12]. Computed tomography (CT) is a method that can create full 3D reconstructions of samples and should be an ideal method to inspect small joints during the development phase. However, CT experiences difficulties when characterising materials with significant differences in attenuation (such as metals and composites) [13]. A possible solution to this could be the use of dual-energy computed tomography (DECT) that uses the combination of two X-ray spectra's to form an enhanced 3D volume. There are several ways to perform DECT with simple, linear fusions, to more complicated non-linear methods [14, 15, 16].

In this work aluminium–CFRP joints were fabricated and investigated using DECT. The joints were fabricated as integrated double-lap joints with a metal insert embedded in CFRP. The metal inserts were fabricated by milling and AM. The AM metal inserts were both flat and with teeth designed to hook into the CFRP. The teeth were designed to be able to be fabricated in several orientations in the AM process to increase to flexibility of the design (as pins can generally only be fabricated in one orientation). The joints were subjected to mechanical testing in the form of four-point bending and tensile tests. The aim of this work was to investigate and compare the performance of milled/AM joints and to characterise the joints with DECT to explain their behaviour.

2. Materials and methods

This section is divided into four parts. The first describes the design of the metal side of the joints, and the layup of the CFRP. The second describes how the joints were mechanically tested. The third how a simplified simulation of the joints behaviour was conducted. The simulation was performed to acquire information about the general stress distributions in the joint interfaces to be able to discuss the mechanical test results. Finally, the DECT method used to investigate the samples is presented.

2.1. Designs

Three different metal inserts for metal-composite double-lap joints were fabricated using two different designs. All the metal inserts were fabricated in aluminium. The first two metal inserts were designed as flat inserts. One fabricated through milling with a sandblasting surface treatment, and one fabricated using selective laser

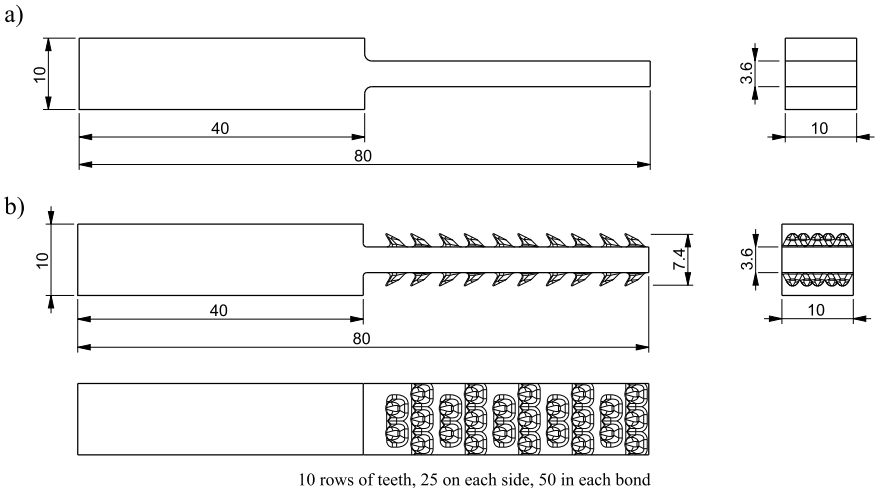

Figure 1. Designs of the metal-inserts for the metal-composite joints: a) The flat inserts; b) The inserts with teeth. All dimensions are given in mm.

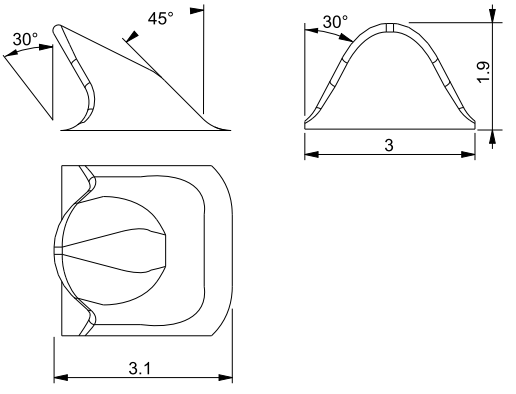

Figure 2. The design of the protruding teeth found on the AM samples. All dimensions are given in mm.

melting (SLM) in the machine EOS 280M. The last bond was also fabricated in the EOS 280M, this bond was designed with 50 small teeth on the surfaces. The parts fabricated with AM did not receive any surface treatment. The designs can be seen in Figure 1. The general design of the teeth can be seen in Figure 2.

All of the samples were fabricated to be 16 mm wide before final processing, this was done to reduce edge effects in the final production process. The fabricated metal inserts can be seen in Figure 3. The specimen types will hereafter be referred to as: Milled, AM, and AM-t (-teeth).

The metal inserts were bonded to the carbon-fibre composite through wet layup. The composite was made up of 50 layers in total, alternating between woven plies of $+90°/0°$ and $+45°/-45°$ orientation. The carbon-fibres used were Torayca® T 300–12000 and the resin was NM 650 epoxy (A bisphenol F resin). Curing was performed under vacuum for 24 hours at 21 °C followed by 24 hours of curing at

 https://doi.org/10.1016/j.heliyon.2019.e01200

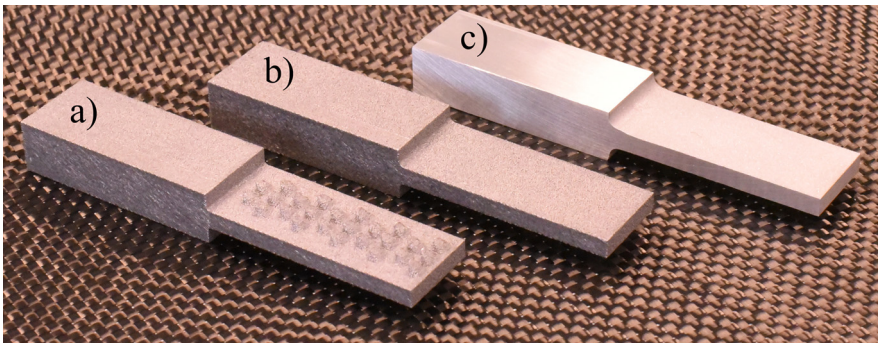

Figure 3. The aluminium side of the three types of bonds studied in this work: a) Metal insert fabricated with AM containing "teeth" on the surface (AM-t); b) Metal insert with a flat surface, fabricated by AM (AM); c) Metal insert with a flat surface, fabricated with milling and sandblasting (M).

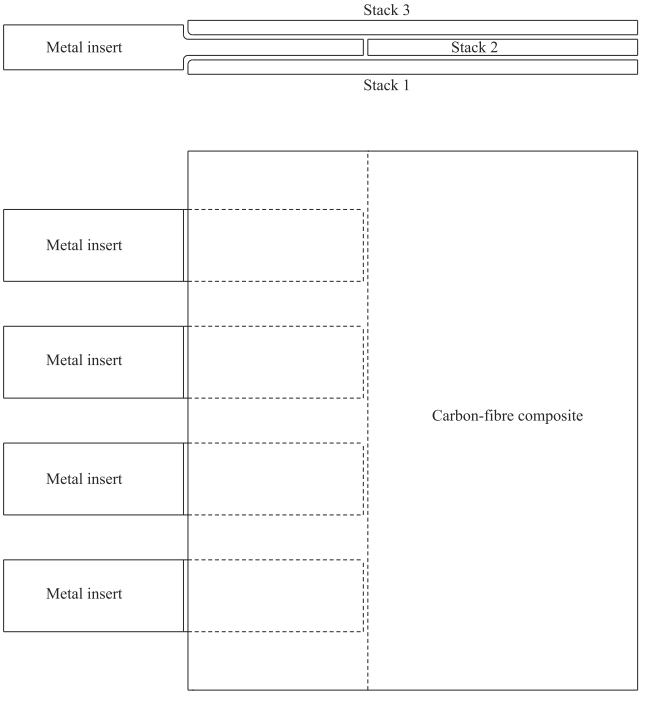

Figure 4. The lay-up method for the samples. Fours samples were cured at the time. First, stack 1 was laid down using wet lay-up, the metal inserts were then pushed into this block while stack 2 was added. Finally stack 3 was added and the lay-up was packaged in release-film, bleeder, and vacuum film.

50 °C. The samples were embedded and cured with four metal inserts per curing, the method of the lay-up can be seen in Figure 4.

After curing the samples were milled to final dimensions. The bars fabricated for tensile testing also had aluminium plates glued to the composite side to prevent damage from the tensile machine grips to the composite during testing. The final dimensions of the test specimens were 120 × 10 × 10 mm, and 155 × 10 × 10 mm, the finished samples can be seen in Figure 5.

https://doi.org/10.1016/j.heliyon.2019.e01200

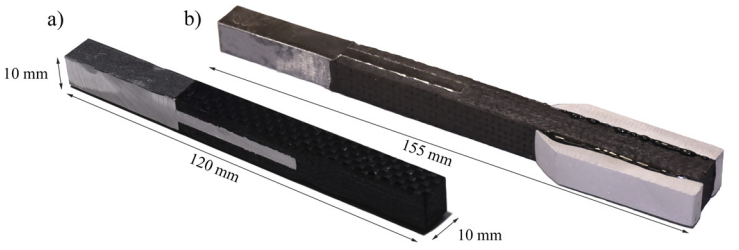

Figure 5. The finished samples after curing and milling to final dimensions: a) Sample for bend testing; b) Sample for tensile testing.

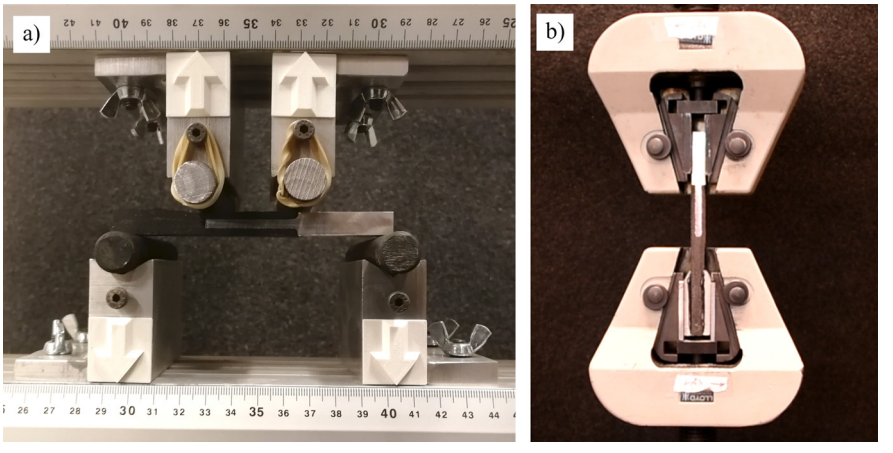

Figure 6. a) The four-point bending setup with a sample mounted. During testing the load is applied by the upper supports. b) The tensile test setup with a sample mounted.

2.2. Mechanical testing

Half of the specimens were evaluated for their bending strength, four of each sample type. The bending was performed using a four-point bending setup. The bend test was chosen to evaluate the samples resistance to peel stress. The loads were applied at the edges of the bond (40 mm apart) so that a constant moment acted on the entire bonded area. The supports were placed 5 mm from the edge of the samples at each side. The bend tests were performed in an Instron 4486 tensile machine. Four samples of each type were also tensile tested in a Lloyd LR 50K. The testing setups can be seen in Figure 6.

2.3. Simulation

The behaviour of the interaction region of the joints were simulated using a simple model in Abaqus [17]. The purpose of this model was not to correctly capture the fracture of the samples but merely to give a hint as to how the stress is initially distributed in the interface between the metal and CFRP during loading. The model assumes the aluminium to have homogeneous material properties with a stiffness

https://doi.org/10.1016/j.heliyon.2019.e01200

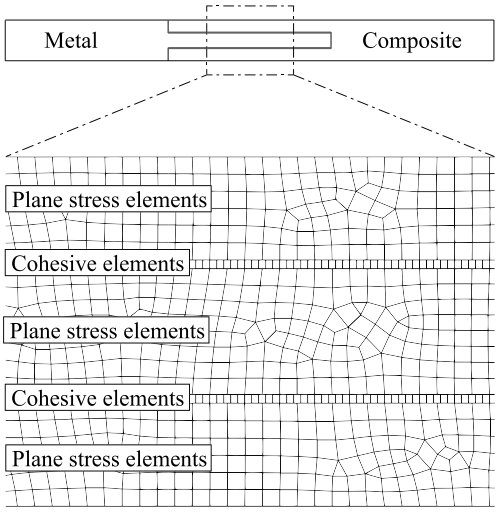

Figure 7. FEM model of a simplified joint. The model uses cohesive elements in the interface region.

Table 1. Energy settings used for the CT scans.

	Voltage (kV)	Current (um)	Filter
High Energy	68	84	None
Low Energy	61	64	None

of 70 GPa while the composite was modelled as an anisotropic material with an in-plane stiffness of 120 GPa and an out of plane stiffness of 14 GPa. On each side of the metal insert there was a region modelled to be the interaction region. This region was modelled to be 250 μm thick with and in plane stiffness of 75 GPa and an out of plane stiffness of 14 GPa. Roughly 400 elements were used for the cohesive region. This model was developed to be similar to previous works on adhesive joints [18, 19]. The model can be seen in Figure 7.

2.4. Dual-energy computed tomography

From each batch of samples (Milled, AM, AM-t) one of the specimens were investigated with CT prior to the mechanical testing to study the metal-composite interface. The specimens were scanned using a sequential acquisition DECT method with two spectra, and a tungsten target in the Nikon XT H 225 system. The acquisition energies can be seen in Table 1.

Each scan had 1440 projections acquired with a 1 s exposure time. The DECT method used in this work is non-linear and was previously presented in [14, 20]. In this method, projections are fused pre-reconstruction by applying a template

https://doi.org/10.1016/j.heliyon.2019.e01200

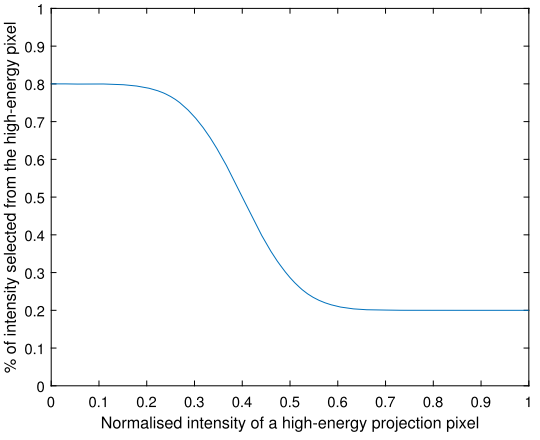

Figure 8. The fusion template function used for the DECT fusion in this work. The function controls how much intensity that is selected from the high, and low, energy projections.

calculated from normalised, high-energy projections. The method fuses the projections using equation (1)

$$I_f = \Delta_{fusion} I_H + (1 - \Delta_{fusion}) I_L, \tag{1}$$

where I_f is a fused pixel, I_H a high energy pixel, Δ_{fusion} value from the template (ranging from 0 to 1), and I_L a low energy pixel. The template was calculated using the normalised high-energy projection for each angle using equation (2):

$$I_N(x, y) = \frac{I_H(x, y)}{max(I_H)}. \tag{2}$$

The fusing template was generated using a sigmoid function which can be seen in Figure 8.

The function was generated from equation (3):

$$\Delta_{fusion} = 0.5 - \epsilon \, \mathbf{erf}(\tau(I_N - \lambda)), \tag{3}$$

where ϵ controls the level of the transition, τ the gradient, and λ where in the grey-scale the transition is centred. In this work the values of the parameters were set as: $\epsilon = 0.3$, $\tau = 7.5$, and $\lambda = 0.4$. The fused projections were reconstructed and analysed in VGStudio MAX [21].

3. Results

This section starts with results from the CT investigations of the samples. This is followed by the results from the mechanical bending, and tensile tests.

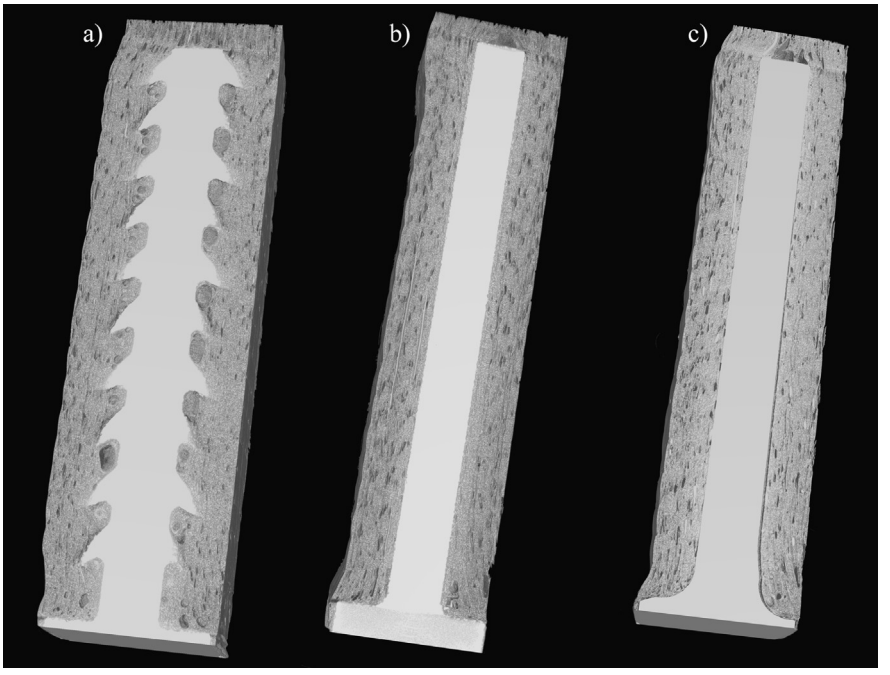

Figure 9. Results from the CT scans of the samples. a) Displays the AM bond containing the teeth. As can be seen, there are issues with the penetration into the fibre plies and there is significant porosity in the epoxy matrix close to the metal. b) The flat AM samples. The data indicates no problems with the adhesion of the matrix to the metal. c) The milled and sandblasted bond, displaying complete loss of adhesion on one side due to damage.

3.1. Computed tomography results

3D cross-sections from each sample type can be seen in Figure 9. The cross-sections are taken from a representative slice of the samples.

As can be seen from Figure 9 (a) there are issues with the penetration of the teeth in AM-t sample into the fibre plies. Severe porosity can be observed in the AM-t sample in the interface between the metal and the composite. For the AM sample the interface between the metal and the composite appears to be well developed. In the milled sample that was scanned one side of the composite had lost contact with the metal insert. A closer look at the interface (on the undamaged side) in the milled sample can be seen in Figure 10.

As can be seen from Figure 10, the interface between the metal and the composite is mostly well developed. The thickness of the interface, defined as the distance between the solid metal to the fibre-plies in the composite, was measured to be around 50 μm. A closer view of the AM sample interface can be seen in Figure 11.

 https://doi.org/10.1016/j.heliyon.2019.e01200

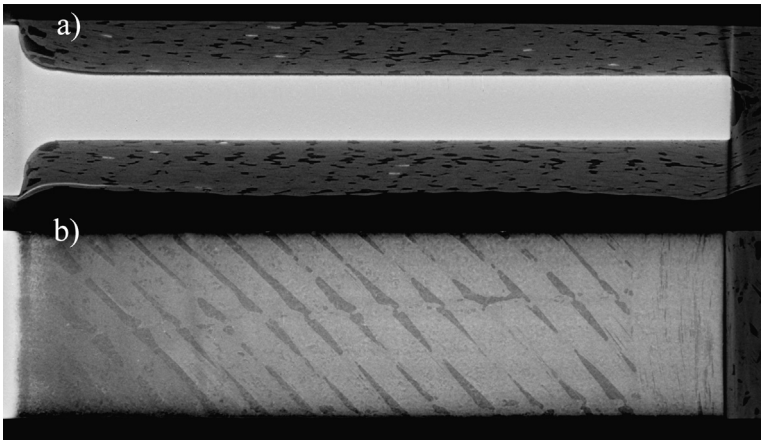

Figure 10. Interface of the milled sample: a) Side view of the joint, if studied closely it can be seen that a section of the top CFRP has lost connection with the metal insert. Except for that part the bonding between the composite and the metal insert looks secure; b) Top view of the interface between the composite and the metal, showing no signs of porosity or delamination.

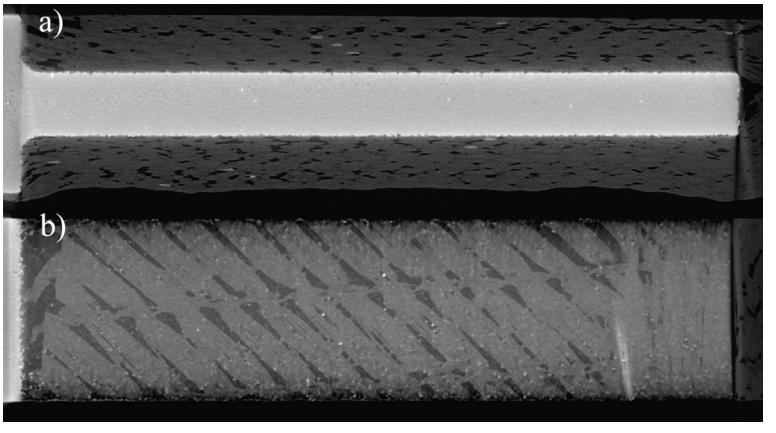

Figure 11. Interface of the AM sample: a) Side view of the joint, the composite appears to be fully connected to the metal. b) Top view from the centre of the interface region. The white spots are metal from the rough AM surface.

The interface region in the AM samples were approximately 260 μm thick, from the valleys of the AM surface to the peaks that were slightly embedded into the composite plies. A closer view of the AM-t sample can be seen in Figure 12.

It is difficult to measure an interface region of the AM-t sample as the entire height of the teeth could be considered to be the interface region. From the CT images there are clearly two different parts to this interface, the first part is where there is only epoxy and teeth present, this region has a highly porous epoxy matrix and is approximately 1.45 mm thick. The second part of the interface consist of the tips of the teeth embedded into the fibre plies, this region has apparently little porosity and is approximately 450 μm thick.

 https://doi.org/10.1016/j.heliyon.2019.e01200

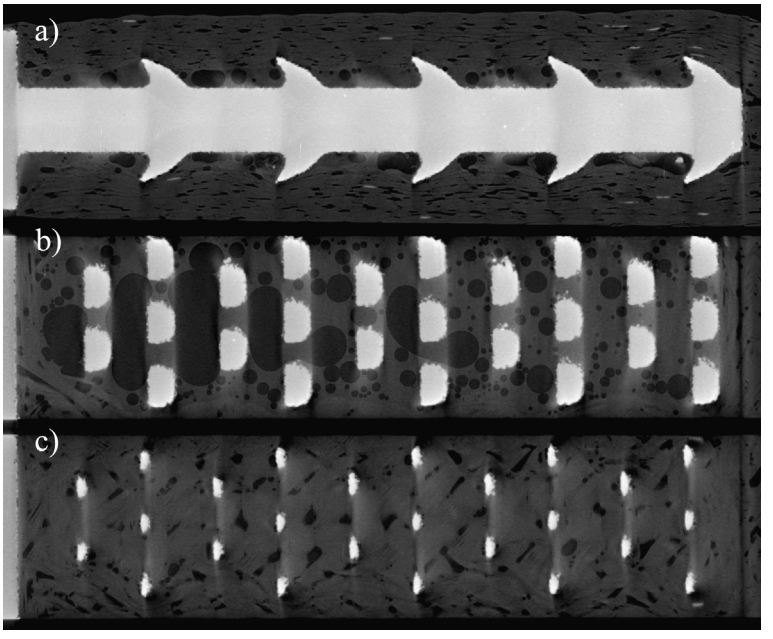

Figure 12. Interface of the AM-t sample: a) Side view of the joint displaying the teeth penetration into the fibre plies and the porosity in the interface; b) Top view of the joint close to the metal, displaying severe porosity in the epoxy matrix and a complete lack of fibres; c) Top view of the joint close to the tip of the teeth, showing that the teeth has some penetration into the fibre plies.

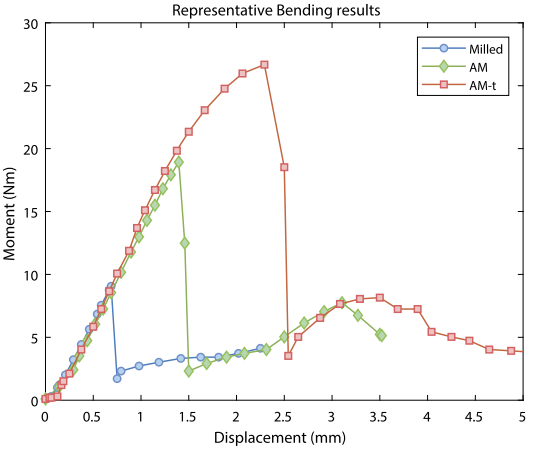

Figure 13. Characteristic bending results from the milled, AM, and AM-t samples.

3.2. Mechanical properties

The milled sample that was scanned was not included in the mechanical properties results as it displayed highly deviating results (because of having a damaged interface). Four samples of each joint type were four-point bend tested and characteristic results can be seen in Figure 13.

 https://doi.org/10.1016/j.heliyon.2019.e01200

Table 2. Average results from four-point bending test for the twelve samples that were evaluated.

Sample	Avg. Max moment	std.	Disp.	std.
Milled	7.1 Nm	1.7 Nm	0.8 mm	0.1 mm
AM	20.2 Nm	1.5 Nm	1.4 mm	0.1 mm
AM-t	29.7 Nm	2.6 Nm	2.3 mm	0.2 mm

Figure 14. Samples after the bend test: a) A milled sample; b) A AM sample; c) A AM-t sample. The samples are seen as they were placed in the testing equipment. The topside of the samples was faced upwards during testing.

Average bending results from all 12 samples can be seen in Table 2. One of each of the broken samples can be seen in Figure 14.

From the results it can be seen that each group of samples has a clearly distinguishable behaviour. The weakest specimens were the milled samples that failed in the elastic region. The AM samples could withstand 285% more load than the milled samples. Again, the samples failed in the elastic region. Finally, the AM-t samples could withstand 418% more load than the milled samples. For the AM-t samples the failures appear to have occurred in a plastic region. All of the samples failed when the composite on the lower face of the metal lost contact with the metal insert.

The results from the tensile tests can be seen in Figure 15, and Table 3.

From the tensile results it can be seen that all of the specimens fail in a plastic region. The milled, and AM samples, fail at approximately the same loads and displacement while the AM-t sample fail at a lower load.

 https://doi.org/10.1016/j.heliyon.2019.e01200

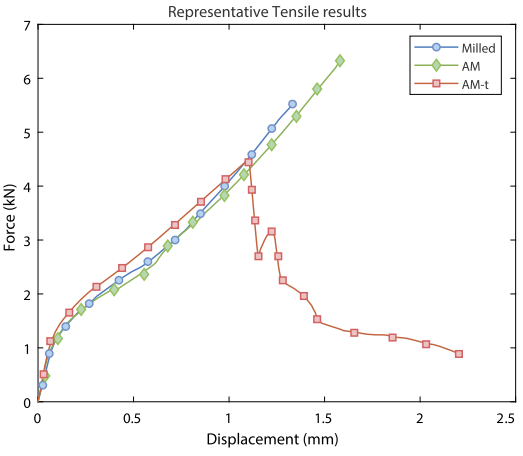

Figure 15. Characteristic tensile results from the milled, AM, and AM-t samples.

Table 3. Average results from the tensile test on the specimens.

Sample	Avg. Max force	std.	Disp.	std.
Milled	6.5 kN	1 kN	1.5 mm	0.2 mm
AM	6.6 kN	0.3 kN	1.4 mm	0.2 mm
AM-t	4.5 kN	0.6 kN	1 mm	0.1 mm

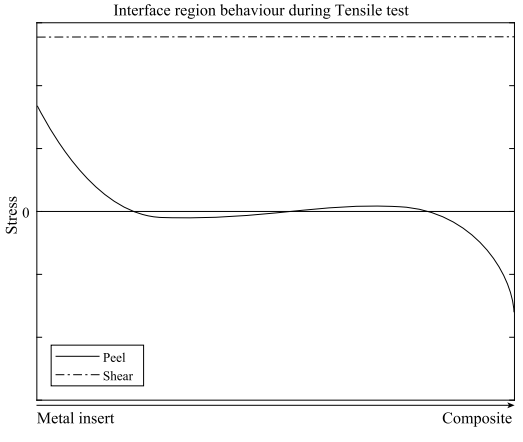

Figure 16. Simulation results of the peel, and shear, stress distribution in the interface region during tensile testing.

3.3. Simulation

The results from the FEM simulations are presented as the stress distribution in the interface region between the metal insert and the composite. A positive peel stress indicates that the composite is being peeled away from the metal insert for both the upper, and lower, interface region. The simulation of the tensile test can be seen in Figure 16.

 https://doi.org/10.1016/j.heliyon.2019.e01200

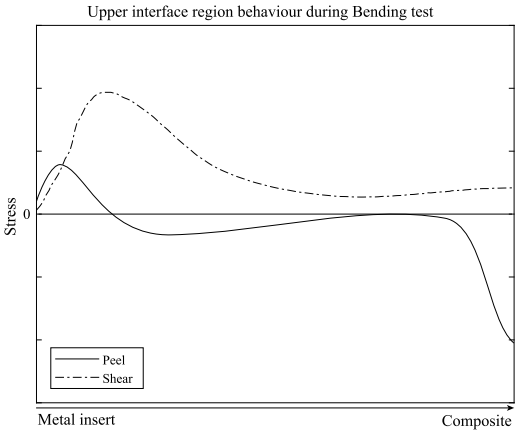

Figure 17. Simulation results of the peel, and shear, stress distribution in the upper interface region during four-point bending.

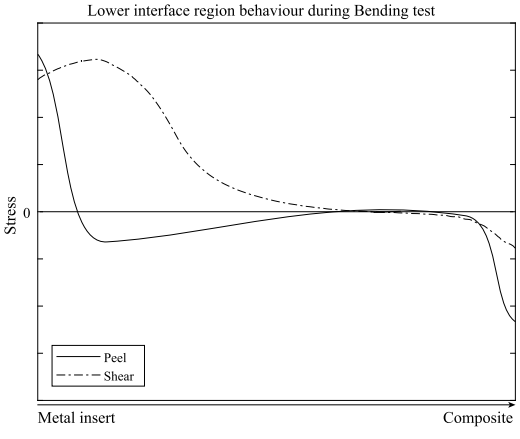

Figure 18. Simulation results of the peel, and shear, stress distribution in the lower interface region during four-point bending.

Since it is a symmetrical load case the behaviour of both interface regions is the same with an almost constant shear-stress. The peel-stress causes the material to peel of closest to the metal insert and pinch around it at the composite end. The result for the upper interface region during four-point bending can be seen in Figure 17.

From the simulation it can be seen that the peel stress that wants to remove the composite from the metal has approximately half the magnitude of the shear stress. In the composite end of the joint the composite is pinched down around the metal insert. The result from the lower interface region can be seen in Figure 18.

From the simulation of the lower interface region it can be seen that the peel stress is of equal magnitude to the shear stress at their maxima's. The highest peel stress is found closest to the metal side of the bond and is likely the limiting factor in this load case.

4. Discussion

The severe porosity in the AM-t samples was caused by the inability of the teeth to penetrate the plies, leaving pockets of air beneath the teeth (Figure 12 b)–c)). The air pockets were not removed during the curing of the parts and as a result the interface between the metal and the composite was negatively impacted. From the CT results it can be estimated that the absence of epoxy in the interface of the AM-t bond could be as much as 20–30%. It is possible that the use of an ultrasonic horn to vibrate the teeth into the fibre plies prior to curing could have improved the bonding significantly [3]. Future work should include detailed studies of the fabrication process of these types of joints to find suitable methods to maximise the strength of the bond.

In the AM, and Milled, samples the interfaces appeared much the same in terms of porosity as there was hardly any to be found (except for on the damaged side of the Milled sample). The difference between the specimens was the thickness of the interaction zone between the metal and the composite. The interface in the AM samples was roughly 500% thicker than the Milled samples.

The bending results can partly be explained by these interaction zones. In the bending tests it could be seen from the simulations (Figure 18) that a significant amount of peel stress is to be expected on the bottom side of the joints. This caused all of the joints to fail to an adhesive failure between the metal and the composite, starting from the metal insert side (Figure 14). Having an interface with a rough metal surface protruding into the fibre plies should be beneficial to carry peel stress compared to not having it (AM vs Milled). The increased surface area alone allows for greater adhesion strength while there is also a chance that fibres can wrap around surface formations, providing an additional mechanical bond. Further, having teeth protruding into the plies should be more beneficial than only having a rough surface (AM-t vs AM). In addition to the previously mentioned mechanisms these joints have an even greater surface area as well as a high chance for mechanical bonding as the fibres wrap around the surface features. This reasoning seems to explain the results from the mechanical tests.

As for the tensile strength of the samples it can be seen from the simulation that the majority of the load is transferred through shear. In shear, the area of the interaction zone is the major factor to the strength of the joints. All of the bonds had cohesive failures and thus the major factor to how much load they could carry was the area of the interaction zone. As could be expected from the CT data, the AM and Milled samples had similar load bearing capacity since they both had the same interaction zone area. The AM-t bonds, however, were weaker in this loading situation since the porosity in the interaction zone gave them a smaller bonding area (Figure 12 b)–c)). The ability to withstand peel stress has a low significance in tensile loading and thus the teeth had little effect until after initial failure.

 https://doi.org/10.1016/j.heliyon.2019.e01200

The DECT method produced great results for investigation of the bonds that made it possible to understand their complex behaviour during loading. Possibly, the method could have produced even greater results if there had been a greater difference between the energy levels used for the scans (the composite could have benefited from a lower energy), however, this was not possible in the CT system used for this study.

To fully understand the behaviour of these types of joints it is important to understand the behaviour of the surfaces themselves. In the AM community the study of surfaces is a topic of high interest and recent research indicates that since the surfaces are micro-porous they need to be investigated with CT to capture their complete morphology [22, 23, 24]. Future work on these joints should include detailed studies of the AM surfaces where the surface energy and permeability are studied in detail for different materials and build orientations. The raw data required to reproduce these findings are available by contacting the corresponding author to facilitate data transfer.

5. Conclusion

In this work, three types of double lap joints between aluminium and carbon-fibre composite was studied. The joints examined were fabricated using AM and milling. One of the joints contained teeth designed to hook into the fibre plies of the composite. The bonds were characterised using a non-linear DECT technique which revealed information about the joints metal-composite interfaces.

It was found that joints fabricated with AM was in general stronger in bending because of an increased interface region compared to milled samples. This is due to the inherent rough surface produced by the SLM method. Even though the teeth in the AM samples did not penetrate well into the fibre plies they penetrated enough to increase the joints strength against pull-out, enhancing the bending strength. The tensile tests in this study all led to a cohesive failure in the adhesive, thus the surface roughness of all samples was enough to prevent adhesive failure. The AM joint with teeth was the weakest in tensile loading because of the severe porosity in the joint.

The information gained with the use of DECT was highly valuable as the behaviour of the joints would have been difficult to explain without the porosity information.

 https://doi.org/10.1016/j.heliyon.2019.e01200

Declarations

Author contribution statement

Anton Jansson: Conceived and designed the experiments; Performed the experiments; Analysed and interpreted the data; Contributed reagents, materials, analysis tools or data; Wrote the paper.

Lars Pejryd: Conceived and designed the experiments; Analysed and interpreted the data.

Funding statement

This research did not receive any specific grant from funding agencies in the public, commercial, or not-for-profit sectors.

Competing interest statement

The authors declare no conflict of interest.

Additional information

No additional information is available for this paper.

References

[1] V. Fiore, L. Calabrese, E. Proverbio, R. Passari, A. Valenza, Salt spray fog ageing of hybrid composite/metal rivet joints for automotive applications, Composites, Part B, Eng. 108 (2017) 65–74.

[2] M.M. Abdel Wahab, Fatigue in adhesively bonded joints: a review, ISRN Mater. Sci. 2012 (c) (2012) 1–25.

[3] K. Bodjona, L. Lessard, Hybrid bonded-fastened joints and their application in composite structures: a general review, J. Reinf. Plast. Compos. 35 (9) (2016) 764–781.

[4] L. Pejryd, T. Beno, S. Carmignato, Computed tomography as a tool for examining surface integrity in drilled holes in CFRP composites, Proc. CIRP 13 (2014) 43–48.

 https://doi.org/10.1016/j.heliyon.2019.e01200

[5] J. Jahn, M. Weeber, J. Boehner, R. Steinhilper, Assessment strategies for composite-metal joining technologies – a review, Proc. CIRP 50 (2016) 689–694.

[6] F. Smith, Comeld™: an innovation in composite to metal joining, Mater. Technol. 20 (2) (2005) 91–96.

[7] X. Wang, J. Ahn, C. Kaboglu, L. Yu, B.R.K. Blackman, Characterisation of composite-titanium alloy hybrid joints using digital image correlation, Compos. Struct. 140 (2016) 702–711.

[8] P.N. Parkes, R. Butler, J. Meyer, A.D. Oliveira, Static strength of metal-composite joints with penetrative reinforcement, Compos. Struct. 118 (2014) 250–256.

[9] P.N. Parkes, R. Butler, D.P. Almond, Growth of damage in additively manufactured metal-composite joints, in: Eccm15 – 15th European Conference on Composite Materials, June, 2012, pp. 24–28.

[10] D.P.A. Philip, N. Parkes, Richard Butler, Fatigue of metal-composite joints with penetrative reinforcement, in: Proceedings of 54th AIAA/ASME/ASCE/AHS/ASC Structures, Structural Dynamics and Materials Conference, 2013, pp. 1–8.

[11] L. Pejryd, P. Karlsson, S. Hällgren, M. Kahlin, Non-destructive evaluation of internal defects in additive manufactured aluminium, World PM 1 (2016) 1–6.

[12] S. Gholizadeh, A review of non-destructive testing methods of composite materials, Proc. Struct. Integrity 1 (2016) 50–57.

[13] L. De Chiffre, S. Carmignato, J.-P. Kruth, R. Schmitt, A. Weckenmann, Industrial applications of computed tomography, CIRP Ann. 63 (2) (2014) 655–677.

[14] A. Jansson, J. Ekengren, A.-R. Zekavat, L. Pejryd, Effects of X-ray penetration depth on multi material computed tomography measurements, in: 6th Conference on Industrial Computed Tomography, 2016, 8 pp.

[15] M. Krumm, S. Kasperl, M. Franz, Reducing non-linear artifacts of multi-material objects in industrial 3D computed tomography, NDT E Int. 41 (4) (2008) 242–251.

[16] P. Krämer, A. Weckenmann, Multi-energy image stack fusion in computed tomography, Meas. Sci. Technol. 21 (4) (2010), 7 pp.

[17] Abaqus/CAE, 2017.

[18] U. Stigh, A. Biel, T. Walander, Shear strength of adhesive layers – models and experiments, Eng. Fract. Mech. 129 (2014) 67–76.

[19] X. Hou, A. Yousefi Kanani, J. Ye, Double lap adhesive joint with reduced stress concentration: effect of slot, Compos. Struct. 202 (2018) 635–642.

[20] A. Jansson, L. Pejryd, A dual-energy approach for improvement of the measurement consistency in computed tomography, Meas. Sci. Technol. 27 (11) (2016), 9 pp.

[21] VGstudio MAX 3.0, 2016.

[22] G. Kerckhofs, G. Pyka, M. Moesen, S. Van Bael, J. Schrooten, M. Wevers, High-resolution microfocus X-ray computed tomography for 3d surface roughness measurements of additive manufactured porous materials, Adv. Eng. Mater. 15 (3) (2013) 153–158.

[23] A.R. Zekavat, A. Jansson, C. Gundlach, L. Pejryd, Effect of X-ray computed tomography magnification on surface morphology investigation of additive manufacturing surfaces, in: iCT 2018, iCT, 2018, pp. 1–7.

[24] A. Townsend, R. Racasan, R. Leach, N. Senin, A. Thompson, A. Ramsey, D. Bate, P. Woolliams, S. Brown, L. Blunt, An interlaboratory comparison of X-ray computed tomography measurement for texture and dimensional characterisation of additively manufactured parts, Addit. Manuf. 23 (2018) 422–432.